Journal of Electrostatics 89 (2017) 77–87

Contents lists available at ScienceDirect

Journal of Electrostatics

journal homepage: www.elsevier.com/locate/elstat

# Modeling simple-jet mode electrohydrodynamic-atomization droplets' trajectories and spray pattern for a single nozzle system

O.M. Ondimu [a, b, *], V.A. Ganesan [d], M.J. Gatari [a], J.C.M. Marijnissen [a, c], L.L.F. Agostinho [b, c, d]

[a] Institute of Nuclear Science and Technology, University of Nairobi, Nairobi, Kenya
[b] Centre of Expertise Water Technology, Leeuwarden, 8934CJ, The Netherlands
[c] Wetsus, Leeuwarden, 8911MA, The Netherlands
[d] NHL University of Applied Sciences, Water Technology Research Group, Leeuwarden, 8917DD, The Netherlands

ARTICLE INFO

*Article history:*
Received 13 February 2017
Received in revised form
24 July 2017
Accepted 9 August 2017

*Keywords:*
Droplet trajectories
Electrohydrodynamic atomization (EHDA)
Electrospraying
Modeling
Simple-jet mode

ABSTRACT

Electrohydrodynamic atomization (EHDA), or simply Electrospraying is the process of influencing the breakup of a liquid into droplets by using a strong electric field. There can be different modes of Electrospraying depending, basically, on the created electric field strength and the liquid flowrate, for a specified liquid. Among these modes, the so-called cone-jet mode is the most explored one. This is due to its ability to produce highly charged monodisperse droplets in the nano- to micro-meter size range. Another mode of interest, which can also produce monodisperse droplets is the simple-jet mode. This mode is less explored when compared to the former. Within the papers that were explored by the authors, Agostinho et al. (2012) were the first authors to carefully investigate and characterize this mode. In their work, the authors reported about the influence of the electric field and the liquid flowrate on the droplets' size and spray dispersion. They also pointed out that the charge on these droplets can be expressed as a certain percentage of their Rayleigh limit.

So far, there has been no model proposed to describe the droplets' trajectories in the simple-jet mode. This paper describes the design and the implementation of a physical model for determining the droplet trajectories in this mode. The model is done, specifically, for a single nozzle/ring-up configuration. It is a two-dimensional model, which solves the force balance equation for each droplet breaking up from the jet. It takes into consideration; the initial droplet velocity, the force of gravity, the electric field force, the inter-droplet coulombic force and the drag force. The droplets' deformation and reorientation were hypothesized, from observations, to play a major role in initiating the droplets' dispersion. They were simulated by implementing periodic displacements on the droplets' center of charge from its center of mass. The calculated droplets' trajectories' envelope angle was fitted to the experimental envelope angle by adjusting the droplet charge around the values that were reported by Agostinho et al. (2012). The model was validated by comparing the shapes of the theoretical and experimental sprays.

The model offers new possibilities of modeling the droplets' trajectories in complex geometries, and of introducing additional forces to manipulate their trajectories in the simple-jet mode.



## 1. Introduction

Electrohydrodynamic Atomization (EHDA), or simply Electrospraying, is the process of influencing the breakup of a liquid into droplets by using a strong electric field (kV.cm$^{-1}$) [1]. William Gilbert (1600) is the first author to report the effect of a strong electric field on a liquid surface. In his work "*De Magnete*", he noted that when a piece of charged amber is brought close to a liquid droplet standing on a dry surface, it changes its shape from spherical into conical [2]. Since then, many authors have made a lot of contribution into the study of this phenomenon and implemented it in electrospraying [1,3].

In electrospraying, the strong electric field is produced by applying a potential difference between a nozzle and a conductive surface positioned close to it (counter electrode). This is usually performed in three different configurations, i.e. nozzle/ring-up, nozzle/ringdown and nozzle/plate [4]. For each of these

* Corresponding author. Institute of Nuclear Science and Technology, University of Nairobi, P.O. Box 30197-00100, Nairobi, Kenya.
*E-mail address:* obedmarube@gmail.com (O.M. Ondimu).

http://dx.doi.org/10.1016/j.elstat.2017.08.001
0304-3886/

configurations, there are different modes of electrospray, which can be created depending, basically, on the liquid flowrate, electric field intensity, and liquid properties, such as surface tension, electrical conductivity, electric permittivity, viscosity and density [5,6]. Cloupeau and Prunet-Foch (1990) were, probably, the first authors to classify the different electrospraying modes, relying on the morphology of the meniscus and the formed jet [7]. Later on, the same authors, and Grace and Marijnissen (1994) extended the classification further into dripping, spindle, intermittent cone-jet, cone-jet, and the multiple-jet modes; for low flowrates, and the simple-jet mode; for higher flowrates [8,9]. Among all these modes, the cone-jet mode is, so far, the most explored because of its capability of producing highly charged monodispersed droplets in the nano- to micro-meter size range. More information about this mode can be found in the literature [3,10,11].

Many theoretical investigations have also been conducted to predict some of the electrospray characteristics, such as the droplets' movement, the spray pattern, the liquid breakup process, etc. Most of these investigations, however, are done only for the cone-jet mode. Gañán-Calvo et al. (1994) proposed an electrospray model using the Lagrangian model of particle motion [12]. The author used the momentum equation given by Tchen (1947) and Maxey (1983), taking into account four types of forces, namely: gravitational force, electric field force, coulombic force and drag force [13]. Tang and Gomez (1994) modified this model further by calculating the electric field using the measured droplets' velocities [14]. Grace and Dunn (1996) presented a two-dimensional mathematical model to describe the droplet behavior within an electrodynamic fine spray [10]. Later on, Hartman et al. (1999) modeled the Taylor cone and calculated the spray dispersion. Unlike Gañán-Calvo and Tang, Hartman calculated the background electric field using Gauss Law and assumed a smaller radial displacement of the droplets at their region of formation. The author also assumed a bimodal droplet size distribution instead of the lognormal droplet size distribution used by Gañán-Calvo [3]. Later on, Geerse (2003) described a three-dimensional model for predicting the droplet dispersion and the deposition region. He calculated the background electric field using FEMLAB® software package [4]. Grifoll-Taverna, J. and Rosell-Llompart, J. (2009) described a numerical model that predicts the spray characteristics in the same mode, using a nozzle/plate configuration [15].

The simple-jet mode has not been so much explored as the cone-jet mode, both, experimentally and theoretically. However, it is the recommended mode for applications that depend on electrospraying at high throughputs, such as spray drying, and desalination systems [1]. Agostinho et al. (2012) are, probably, the first authors to experimentally analyze and characterize this mode. In their work, the authors defined an operational window for this mode in relation to the electric potential and the liquid flowrate for deionized water. They further investigated the effect of liquid electric conductivity on the spray diagram and found out that it only plays a very small role, concerning whipping and dispersion limits. Additionally, they pointed out that the droplet charge can be expressed as a certain percentage of their Rayleigh limit [1]. The authors, further, presented a simple-jet multi-nozzle system and reported its influence on liquid evaporation [16].

In this work the authors are proposing a physical model which can be used to describe the droplet trajectories in the simple-jet mode. The specified input parameters include: background electric field, droplet initial velocity, droplet size distribution, jet breakup length and droplet charge. These parameters were specified for a given set of liquid flowrate and applied electric potential. The background electric field is calculated using COMSOL Multiphysics® software package. The droplets' trajectories are calculated by solving the force balance equation for each droplet using MATLAB®. The input parameters of the model, as well as the real spray pattern used to validate the model, were obtained by analyzing images taken with a high-speed imaging system.

The model was qualitatively validated by comparing equivalent theoretical and experimental spray shapes, and quantitatively by comparing their axial cross-sectional areas. After validating the model, different components of the forces acting on the droplets were analyzed. This analysis indicated that the coulombic force was the major component contributing to the droplets' dispersion.

The model introduces new possibilities of modeling in more complex geometries and of predicting the kind of extra forces, such as secondary electric field and an airflow, necessary to manipulate the droplets' trajectories in the simple-jet mode.

## 2. Methodology

The adopted method for constructing and validating the model can be resumed in three steps: data acquisition, calculation of the droplets' trajectories, and validation. Data acquisition was done by both calculating the background electric field with COMSOL Multiphysics® software, as well as by experimentally obtaining other input parameters, such as the droplets' initial velocity, droplets' average Feret diameter, droplets' size distribution and the jet breakup length. Sequentially, these input parameters were used to calculate the droplet trajectories and consequently, the spray patterns using MATLAB®. Finally, the model was validated by comparing the theoretical spray patterns to their equivalent experimental spray patterns. This process was done for different values of the liquid flowrate and electric field intensity. In the validation phase, whenever a deviation of more than 10% between the theoretical and experimental spray patterns was found, the droplets' charge was adjusted in the model and their trajectories were calculated again. A more illustrative view of the followed steps is as shown by the fluxogram presented in Fig. 1. A detailed explanation for each step is given in the next section.

### 2.1. Input parameters

The data input part of the model was based on two main steps, i.e. calculation of the background electric field using COMSOL Multiphysics® software, and obtaining the spray/droplets characteristics.

#### 2.1.1. Calculation of the background electric field

The process of calculating the background electric field as a function of the setup geometry, using COMSOL Multiphysics® software package, started by defining the geometry for a single nozzle/ring-up configuration (Fig. 2). This geometry was similar to the one which was used for all the experiments. It is known that the best environment in this case would be a 2D axisymmetric or a 3D. However, as will be also further commented, to take advantage of the known symmetry of EHDA sprays and make the model simpler, the authors decided to opt for a 2D environment. Additionally, the validation technique which was to be used to verify the final trajectories of the droplets was also a two dimensional technique. Therefore, the definition was done using the 2D space dimension package in the electrostatics interface of the software's AC/DC module, for a stationary study scenario. The geometry was defined with a nozzle of outer diameter (OD) of 0.51 mm and an inner diameter (ID) of 0.25 mm. The distance between the nozzle tip and the counter electrode ring was set to 17 mm. Materials were defined using the in-built COMSOL Multiphysics® Material library in the following way: copper was used for the counter electrode ring, stainless steel 405 annealed for the nozzle, FR4 (circuit board) for the counter electrode support, and finally, air was used for the

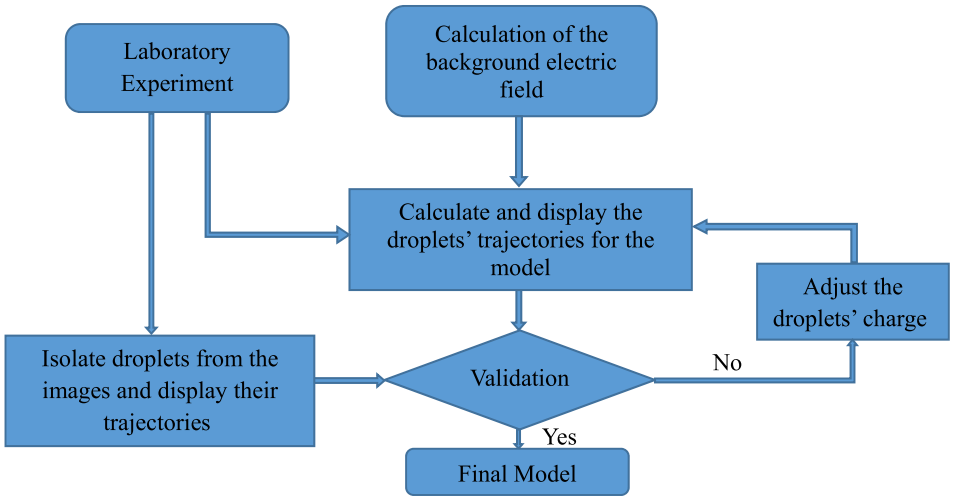


**Fig. 1.** The method fluxogram showing the experimental and the modeling steps followed in this work.

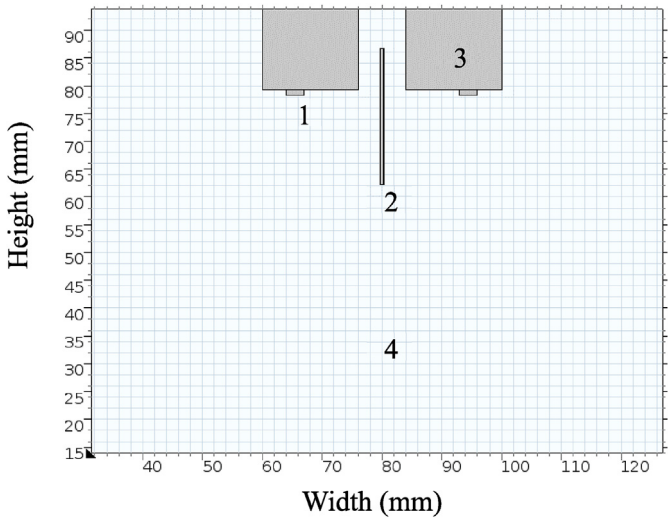


**Fig. 2.** Defined geometry in COMSOL Multiphysics® (counter electrode ring (1), nozzle (2), counter electrode support (3) and surrounding environment (4)).

surrounding environment.

The electrostatics boundary conditions for the geometry were defined as follows: ground for the nozzle (with zero potential), electric potential for the counter electrode (whose value was varied between −5 kV and −9 kV in steps of −1 kV), dielectric shielding for the circuit board and zero charge for the exterior boundaries.

The model was computed for different values of applied electric potential. The obtained results were then exported to MATLAB®, where a self-developed routine was used to extract individual values of the electric field ($E_{x,y}$) at every position inside the geometry.

### 2.1.2. Experimental method

To obtain the input parameters for the model, a single nozzle/ring-up setup was built as shown in Fig. 3 with the same dimensions as highlighted in the previous section. A pump type MasterFlex® Console Drive was used to pump the liquid at a constant flowrate through the nozzle. The liquid used for all the experiments was tap water (properties shown in Table 1).

The experiments were performed with three different the flowrates; 285 mL $h^{-1}$, 360 mL $h^{-1}$ and 440 mL $h^{-1}$, i.e. the jetting regime of droplet formation. The electric potential was applied to the counter electrode (FUG HCP 14-20000 DC high voltage power supply), while the nozzle was kept grounded in all the experiments. The values of the applied electric potential varied between −5 kV and −9 kV in steps of −1 kV for each flowrate.

In order to visualize the droplets and the spray, a high speed imaging system consisting of a Photron® SA-X2 high-speed camera with a NAVITAR® microscopic lens and a Dedocool® backlight illumination was used as shown in Fig. 3.

The images were recorded at a constant frame rate (12500 fps) and then processed using ImageJ® software together with a self-developed MATLAB® routine. This process comprised of obtaining the droplets' size distribution, and shape deformation as well as the jet breakup length. This was followed by isolating the individual droplets and some of their properties, namely: the initial velocity, the Reynolds number, the trajectories, and finally the spray shape used in the validation phase.

## 2.2. Calculation of droplets' trajectories

The calculation of the electrosprayed droplets' trajectories, and hence the spray shape for the model, involved solving the force balance equation (in the x- and y-axes of the geometry) for each droplet breaking up from the jet. This equation takes into consideration the background electric field force ($\vec{F}_E$), the coulombic force ($\vec{F}_C$), the gravitational force ($\vec{F}_g$) and the drag force ($\vec{F}_D$) as shown in equation (1).

$$\vec{F}_{Ri} = q_i.\vec{E} + q_i.\sum_{\substack{j=1\\ j\neq i}}^{N}\frac{q_j.\vec{r}_{ij}}{4\pi\varepsilon_o.r_{ij}^3} + C_D.\frac{\pi}{8}.\rho_{air}.d_i^2.(\vec{v}_{air} - \vec{v}_i).|\vec{v}_{air} - \vec{v}_i| + \frac{\pi}{6}.\rho_i.d_i^3.\vec{g} \quad (1)$$

where: $\vec{F}_{Ri}$ is the resultant force, q is the droplet charge, *i* and *j*, the droplet indices, *r*, the inter-droplet distance, $\varepsilon_o$ is the electric permittivity of free space, $\rho_{air}$ and $\rho_i$, the density of air and droplet respectively, *d* is the droplet's diameter, $\vec{v}_{air}$ and $\vec{v}$, air and droplet's velocity respectively, $\vec{g}$ is the gravitational acceleration and $C_D$ is the drag coefficient, which is calculated depending on the regime in which the droplet was moving. A stagnant air condition

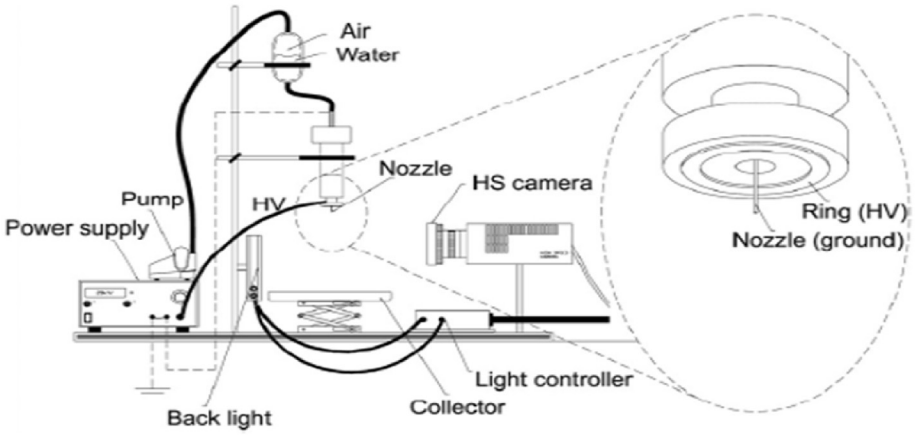


**Fig. 3.** Experimental setup for obtaining initial droplets' condition (Agostinho et al. [1]).

**Table 1**
Properties of the liquid (tap water) used in all the experiments.

| Liquid property | Viscosity, μ (N.s.m$^{-2}$) | absolute density, ρ [kg.m$^{-3}$] | surface tension, γ [N.m$^{-1}$] | electrical conductivity, K [S.m$^{-1}$] | relative permittivity, ε |
|---|---|---|---|---|---|
| Value | $1.00 \times 10^{-3}$ | $1.00 \times 10^{3}$ | $7.19 \times 10^{-2}$ | $5.00 \times 10^{-3}$ | $8.01 \times 10^{1}$ |

($\vec{v}_{air} = 0$) was assumed in all calculations.

The regime in which the droplets were moving was defined by using their Reynolds number, calculated as:

$$Re = \frac{\rho_{air} \cdot |\vec{v}_{air} - \vec{v}_i| \cdot d_i}{\eta_{air}} \quad (2)$$

From the Reynolds number calculation it was observed that in all the evaluated situations, the droplets were moving in the Newtonian regime ($Re \geq 1$). Therefore their drag coefficient was calculated as:

$$C_D = \frac{24}{Re} \cdot \left(1 + 0.15 \cdot Re^{0.687}\right) \quad (3)$$

In this case, the droplets were assumed to be perfect spheres and therefore no shape adjustment was done.

A theoretical droplet population was defined with a size distribution similar to the experimentally obtained droplet population. They were then generated randomly and implemented in the model in a time interval similar to what was observed experimentally.

The next step was defining the necessary time interval between the formation of two droplets. This time interval was experimentally defined and used in the model for all tested configurations and denominated as $\Delta T_D$. Once a droplet was generated, its new position was obtained by solving the force balance equation for constant time steps equivalent to one-fifth of $\Delta T_D$. The new droplet was therefore generated after the predecessor droplet(s) was/were moved five steps. The process was repeated for 100 droplets. After that, the spray pattern was obtained by combining the trajectories of all the generated droplets into a single display (plot).

Another important part of the model was to describe the initial displacement of the EHDA droplets. This is a commonly discussed topic by many authors [4,12]. Ganan-Calvo et al. (1994), in his model of the cone-jet mode, mentioned about these random perturbations and claimed that the results were not sensitive to the initial position of droplet seeding, provided that the displacements were smaller than the jet radius. R.P.A. Hartman et al. (1999) observed that in the same mode, below a certain flowrate, these displacements are small, in comparison with the jet radius, for a jet breaking up due to varicose instabilities. However, when the liquid flowrate is increased, kink instabilities become more dominant and hence these random displacements are increased [3]. Both authors implemented a random radial displacement of the droplets in the break-up region, to initiate their dispersion. Geerse K. B. (2003) also attributed the spray formation to changes in the droplets' initial velocity vector as a result of their small displacements.

In the presented model, the above mentioned approaches, i.e. the droplets' random initial displacements, as well as their random initial velocity vector, were implemented. However, this could not provide a plausible spray pattern. Instead, it was observed from the images that the droplets' deformation (Fig. 7) might be the major factor contributing to this gradual displacement from their axial position. To verify this, a simulation of this deformation in the model was done by displacing the droplet's center of charge from its center of mass at a certain frequency, whose approximate value was experimentally derived. This approach provided more plausible results when the theoretical and experimental spray shapes were compared.

The droplet's charge, which best described the spray shape, was expressed as a certain percentage of its Rayleigh limit, i.e. the maximum amount of charge a droplet can withstand before splitting by electrostatic interaction forces [14,17], which is calculated as:

$$q_R = \pi\left(8\varepsilon_o \gamma d^3\right)^{1/2} \quad (4)$$

where: $q_R$ is the Rayleigh Limit, $\varepsilon_o$ is the electric permittivity of free space, $\gamma$ is the surface tension and $d$ is the droplet diameter.

This percentage was firstly assumed to range between 5% and 10%, based on the data presented by Agostinho et al. [18]. However, the final (modeled) value was defined as the value which better described the spray pattern for an approximated axial cross-sectional area of the spray shape, i.e. explained in the next

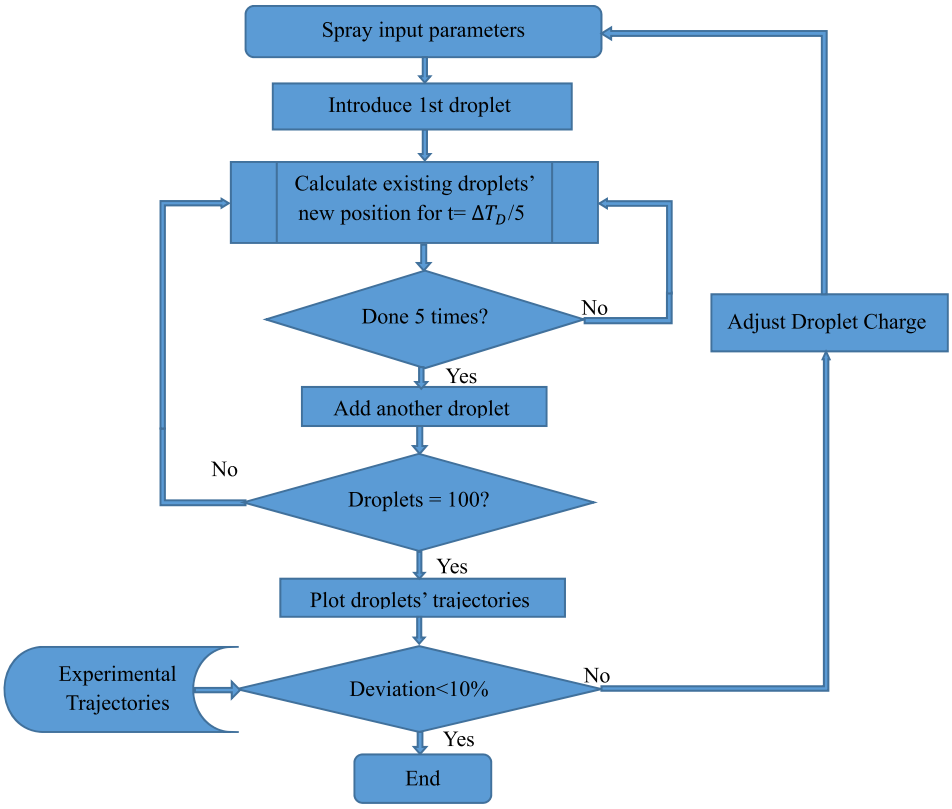


**Fig. 4.** Calculation of the droplets' trajectories for the physical model and validating with the experimental spray shape.

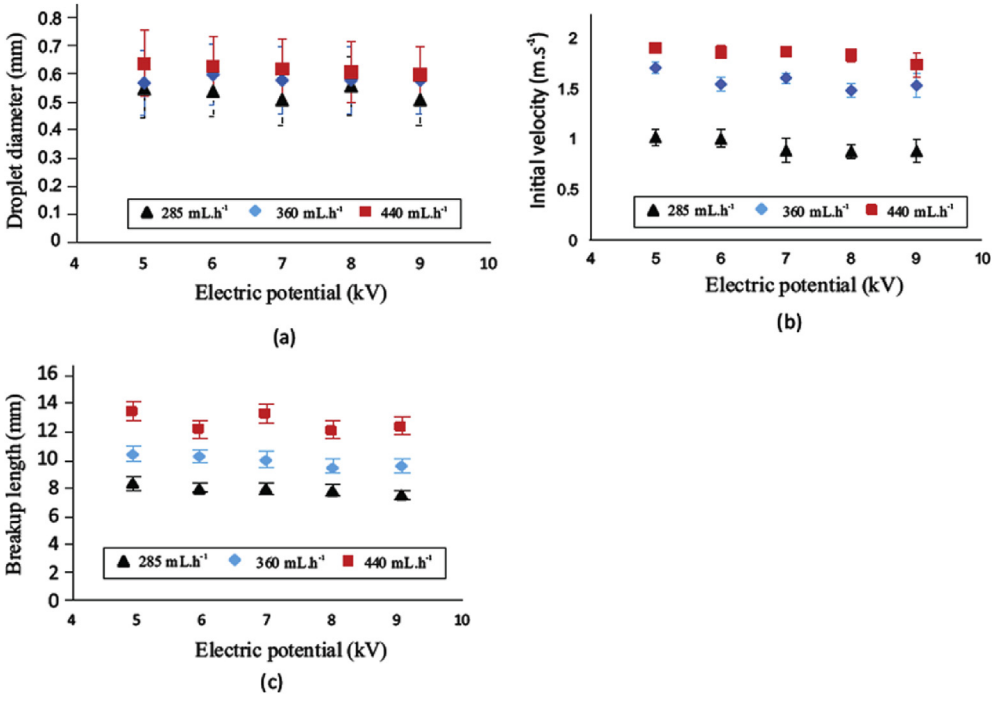


**Fig. 5.** Experimental results for different values of liquid flowrate and applied electric potential; (5a) droplets' average Feret diameter, (5b) droplets' initial velocity, and (5c) jet breakup length. The error bars are representing the standard deviation in the plots, 5a and 5b, and for the plot 5c, an error of 10% was applied.

section. The model has, thus, provided a final droplet charge for every (tested) electric potential and liquid flowrate values which was used as a possible confirmation of the charge percentage for a droplet electrosprayed in the simple-jet mode. The steps which were followed in obtaining and validating the spray shapes are shown in Fig. 4.

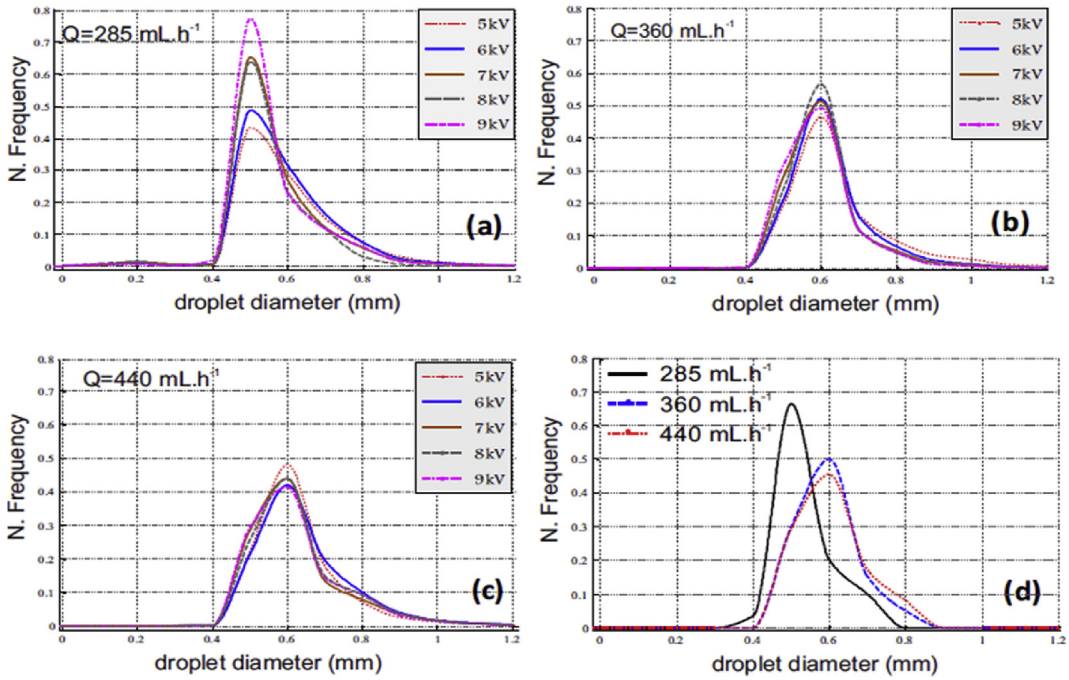


**Fig. 6.** The experimental droplets' size distribution for different values of applied electric potential and different liquid flowrates; (a) flowrate of 285 mL $h^{-1}$, (b) flowrate of 360 mL $h^{-1}$, (c) flowrate of 440 mL $h^{-1}$, (d) simulated droplets' size distribution, for different flowrates.

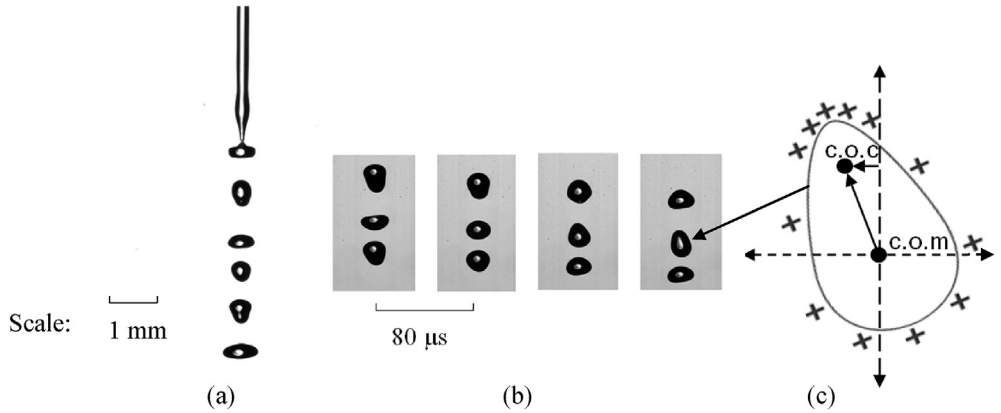


**Fig. 7.** A demonstration of charge displacement by images taken by a high-speed camera at a speed rate of 12500 fps; (7a) A Section of an intact length, with droplets undergoing deformation after they breakup from the jet, (7b) evolution of three droplets in four steps after they breakup from the jet, and (7b) displacement of the center of charge (c.o.c) from the center of mass (c.o.m).

### *2.3. Validation*

The validation phase consisted, basically, on comparing the droplets' trajectories obtained by the model and from the experiments. To facilitate the presentation of the results at this phase, the following denominations will be used throughout the text: (i) the spray "dispersion region", will be used to define the region where the electrosprayed droplets start to be laterally deflected and move off from the spray axis; (ii) the "spray shape" will be used to define the overall spray area. The value of the droplet's charge was adjusted until the spray shape for the model and experiment agreed within an error of 10%.

After the model was validated, different components of the different forces acting on the droplets were analyzed. This was to help predicting the magnitude of possible extra forces required to manipulate the droplets' trajectories.

## 3. Results and discussion

The obtained results from the experiment and the model, as well as the discussions are presented in this section.

### *3.1. The calculated background electric field*

The electric field analysis indicated that for the used geometry, the maximum magnitude of the axial component is generally greater than the radial component. This implies that the droplets will undergo longer axial than radial elongation near the breakup point. This phenomenon of droplets elongation due to an applied electric field has also been reported previously by various authors,

like O'Konski and Taylor [19].

### 3.2. Experimental results and model input parameters

Fig. 5 (a to c) presented below shows the values obtained for the characterization of the droplets average Feret diameter, the jet breakup length and the droplets' initial velocity for all the investigated EHDA settings.

As it can be seen in Fig. 5(a), the droplets' average Feret diameter increases with increasing liquid flowrate, while it only varies slightly with the applied electric potential. This is consistent with the data presented by Agostinho et al. (2013). A direct conclusion is that the liquid flowrate is a more dominant parameter in determining the droplets' size as compared to the applied electric potential, in the case of this mode. Therefore, in the physical model, the average droplet diameter was taken as 0.53 mm, 0.58 mm and 0.62 mm for the flowrates of 285 mL $h^{-1}$, 360 mL $h^{-1}$ and 440 mL $h^{-1}$ respectively.

The results obtained from the investigation of the droplets' initial velocity are shown in Fig. 5(b). From this, it can be seen that the droplets' initial velocity increases with increase in liquid flowrate, but it is not strongly affected by the applied electric potential. Since this value did not change significantly with the applied electric potential, the value of 1.05 m $s^{-1}$, 1.6 m $s^{-1}$ and 1.95 m $s^{-1}$ were used for the flowrates of 285 mL $h^{-1}$, 360 mL $h^{-1}$ and 440 mL $h^{-1}$ respectively.

The results of the jet breakup length measurements are shown in Fig. 5(c). From this figure, it can be seen that the jet breakup length increases with increase in the liquid flowrate, while it decreases slightly with an increase in electric potential. This is also in accordance with Agostinho et al. (2012). In the physical model, it was assumed as the average of all values for different values of applied electric potential, i.e. 8.0 mm, 10.0 mm and 12.0 mm, for the flowrates of 285 mL $h^{-1}$, 360 mL $h^{-1}$ and 440 mL $h^{-1}$ respectively.

The experimental droplets' size distribution was analyzed for the tested applied electric potentials and liquid flowrates. In all the analyses, a total population of droplets ranging between 20,000 and 25000 was considered. Both the experimentally and theoretically defined droplets' population are shown in Fig. 6.

The calculated droplets' relative standard deviation (RSD) was found to range between 0.166 and 0.214. According to Agostinho et al. 2013, an RSD <0.2 indicate a monodisperse size distribution [20].

Fig. 7 shows the droplets undergo vertical and horizontal deformation after breaking up from the jet.

The observation of the images has shown that this deformation has a specific frequency, and is larger in the vertical direction than in the horizontal direction (Fig. 7). This droplets' shape deformation is a well-known subject described by many authors [21,22]. It can be caused by surface waves due to energy release after break up in the case of uncharged droplets [23,24], also due to charge induction/polarization caused by external electric fields, in the case of charged droplets [19,25]. A charged droplet in an electric field, thus, may undergo egg- or tear-shape which would also lead to a non-uniform surface charge distribution.

The non-uniform surface charge distribution on the droplet will cause the displacement of the droplet's center of charge from its center of mass [26] (Fig. 7(c)). The center of charge is displaced to the side of the droplet where the radius of curvature is small, according to the theory of charged spheres [27]. Since all the electric forces acting on the droplet are considered to be concentrated at its center of charge, the droplet will experience a substantial radial component of force due to the electric forces, which will initiate the droplets' displacement from the axial position.

To implement this aspect in the model, the droplet's center of charge was harmonically displaced from its center of mass (Fig. 7(b)), in both the vertical and the horizontal directions.

For the model, it was assumed that the droplets were perfect conductors. This assumption proves to be right, because their charge relaxation time ($\tau = 0.143$ μs) (Eqn. (5)) is much smaller than their period of deformation, which ranges between 480 μs and 641 μs [28].

$$\tau = \varepsilon_0 \varepsilon_r / K \tag{5}$$

In order to find values which could realistically translate the displacements of the droplet's two centers and test the proposed theory, a fitting procedure was defined in the following way. Firstly, the behavior of the sprays droplets was observed for different flowrates and applied electric potential. From these experiments it could be concluded that the produced droplets undergo shape deformation after breakup in a harmonic pattern, i.e. 1560 Hz (for 440 mL $h^{-1}$ and 360 mL $h^{-1}$) and 2080 Hz (for 285 mL $h^{-1}$). After this analysis a specific spray configuration was chosen (285 mL $h^{-1}$ and 5 kV) to be tested in the model. In this test, a displacement of the droplets center was brought to the model at a defined frequency (2080Hz) with different magnitudes for the horizontal and the vertical displacement. For every tested magnitude, the spray dispersion obtained in the model was compared to images taken from experiments using the same flowrate and potential. Two important conclusions were obtained from this first check, namely: (i) the best fit between models and experimental images was obtained when the maximum displacement between the droplets' centers was 60% in the vertical direction and 30% in the horizontal direction (Fig. 8). (ii) When the procedure was repeated for other flowrates and electric potentials, the results showed that these maximum values of displacement remain the same.

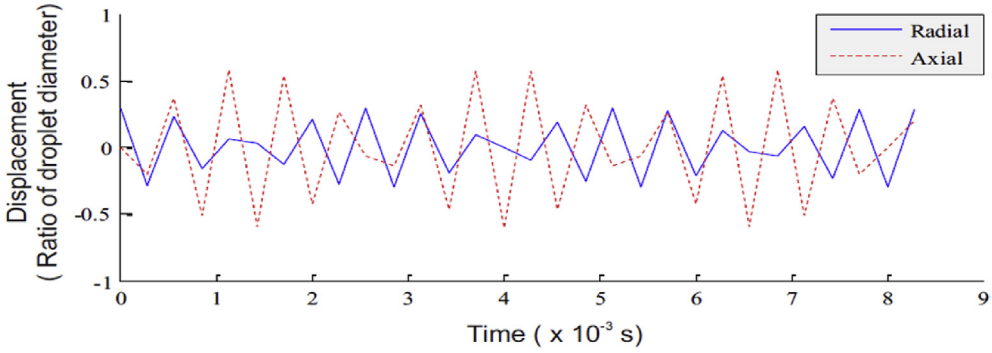


**Fig. 8.** Axial and radial displacement of the center of charge due to droplet's deformation.

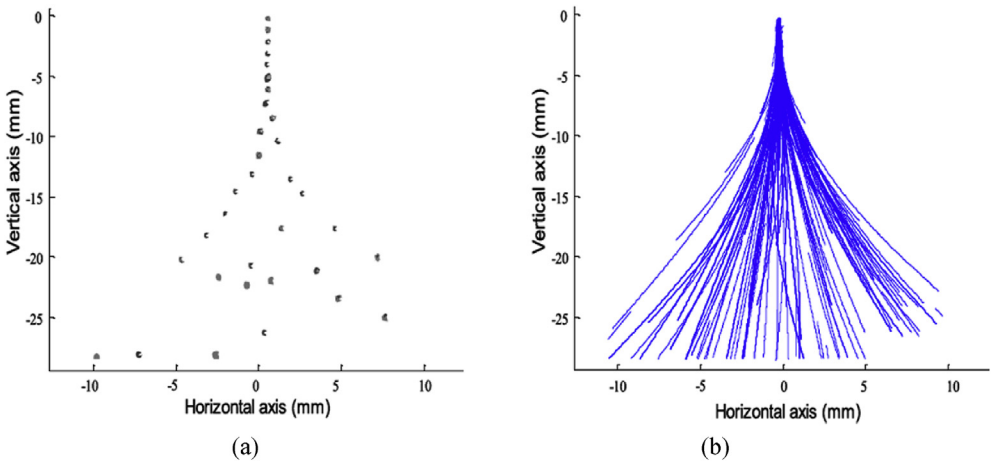


**Fig. 9.** Isolation of individual droplets from the images to obtain the experimental droplets' trajectories: (a) a single image; (b) Experimental droplets' trajectories.

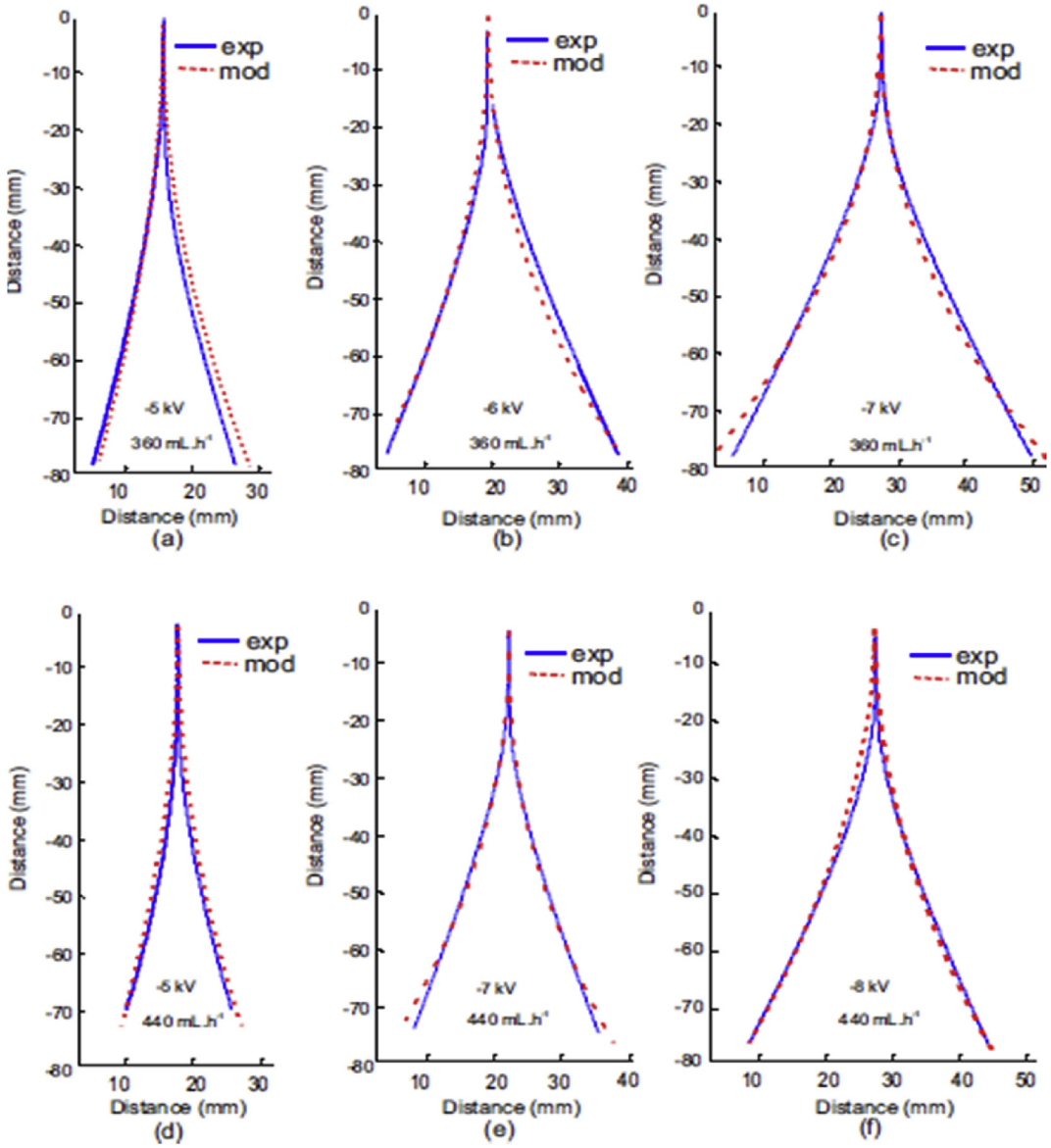


**Fig. 10.** Experimental and calculated droplets' trajectories for some different values of applied electric potential and the liquid flowrate.

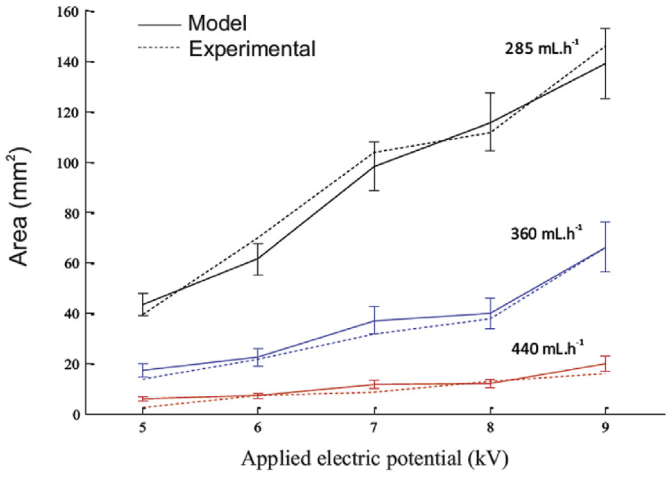


**Fig. 11.** Quantitative Analysis by comparing the theoretical and the experimental spray areas for different values of electric potential, ranging between −9 kV and −5 kV in steps of 1 kV, at the flowrates of 285 mL $h^{-1}$, 360 mL $h^{-1}$ and 440 mL $h^{-1}$.

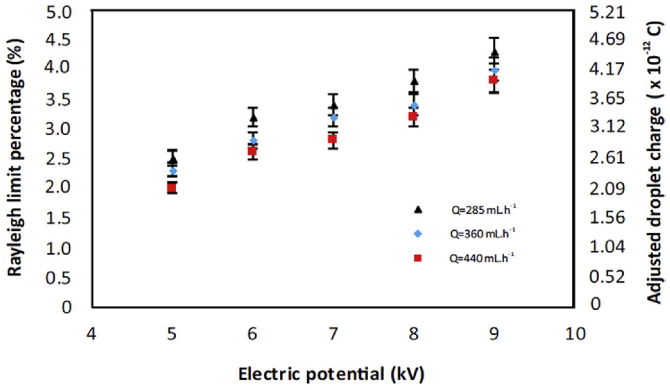


**Fig. 12.** Simulated droplet charge for different values of liquid flowrate and applied electric potential.

During the tests, the observed fact that the droplets deformation was getting damped as they moved away from the break-up point was neglected.

In these tests, the droplets' charge was implemented in the model using the values proposed by Agostinho et al. (2013). However, a second droplet charge check was performed after defining the droplets center's best horizontal and vertical displacement magnitude, by fixing the magnitude and varying the droplets' charge in a close range. This check has clearly demonstrated that, while the "spray dispersion" is highly affected by the magnitude of displacement of the droplets' center of charge, the "spray shape" is more affected by the droplets' charge values. The droplets' charge value tests were repeated for all the tested flowrates and electric potentials and the final results were compared with the values reported by Agostinho et al. (2013).

### 3.3. Experimental droplets' trajectories

Fig. 9 (a) is a representation of a single spray image, and Fig. 9 (b) is a representation of the droplets trajectories after their isolation from the images, using MATLAB®. The spray starts (vertically) from the breakup point, and it's symmetrically presented horizontally i.e., nozzle axis positioned in the x-axis origin. The routine was used to obtain the droplet's velocity, as well as the spray patterns, for different values of applied electric potential and liquid flowrate, which were used for validating the model.

For a more simplified presentation of the validated results, only the trajectories of the external droplets were used to compare the theoretical spray shapes with their corresponding experimental spray shapes. The final images were produced by highlighting the trajectories of the external droplets in both situations (experiment and model) using CorelDRAW® X7, and superimposing them on a Cartesian system (Fig. 10).

Fig. 10 shows that the model successfully describes the spray pattern for the values (tested) of liquid flowrate and applied electric potential. Even though the envelopes are closely similar, they exhibit some unsymmetrical behavior which is attributed to the fact that the routine used in the model to generate the droplets is a random routine, thus, it may generate few droplets which are not the exact size as produced by the real spray. These droplets will, therefore, experience different magnitudes of forces. On the other hand, the small differences between the experimental and theoretical envelopes can be attributed to some factors, such as wind and jet vibrations, which were not accounted for in the model.

A quantitative analysis of the spray shapes was also done by approximating the spray areas to triangles and comparing them. The triangles had their apex located at the breakup point and the bases located at a distance of 18 mm from the breakup point. The results are shown, in Fig. 11.

The plot shows a good agreement between the areas within an error of 10%. It also shows that it decreases with increase in liquid flowrate and increases with increase in applied electric potential.

### 3.4. Droplet charge

The plot presented in Fig. 12 shows the final values of the adjusted droplet charge and their corresponding percentage of the Rayleigh Limit for the tested configurations.

The results show that the droplets' charge increase with an increase in the applied electric potential, and decreases with an increase in the liquid flowrate. It ranges between 2.0% and 4.5% of the droplets Rayleigh limit, for the tested values of liquid flowrate and applied electric potential. These values are close to what was presented by Agostinho et al., 2012. However, independent experiments are recommended to measure the exact charge on the droplets in the Simple-Jet mode, which can be a double-checked with the model.

### 3.5. Representation of all forces acting on the droplets

Fig. 13 (a) shows different forces, decomposed into x (radial) and y (axial) components, acting on a single droplet of 0.741 mm, for an applied electric potential of 5 kV at a flowrate of 360 mL $h^{-1}$.

From the plot it can be seen that the radial component of the electric field force, $\vec{F}_{E(x)}$, is quite small compared with the axial component, $\vec{F}_{E(y)}$, which decreases as the droplets move away from the breakup point. The radial component of the coulombic force, $\vec{F}_{C(x)}$, is much higher than the axial component, $\vec{F}_{C(y)}$, and it almost contributes solely to the resultant force in the x-component, $\vec{F}_{R(x)}$. After decomposing, the axial component of the drag force, $\vec{F}_{D(y)}$, is much higher than the radial component, $\vec{F}_{D(x)}$. This is due to the higher component of velocity in the axial direction as compared to the radial direction.

Fig. 14 shows the normalized weight of the force components for all the considered droplets as the move away from the break-up point.

It is clear from the figure that gravity is the most dominant of all the force components, and its dominance increases with time as the droplets move away from the breakup point.

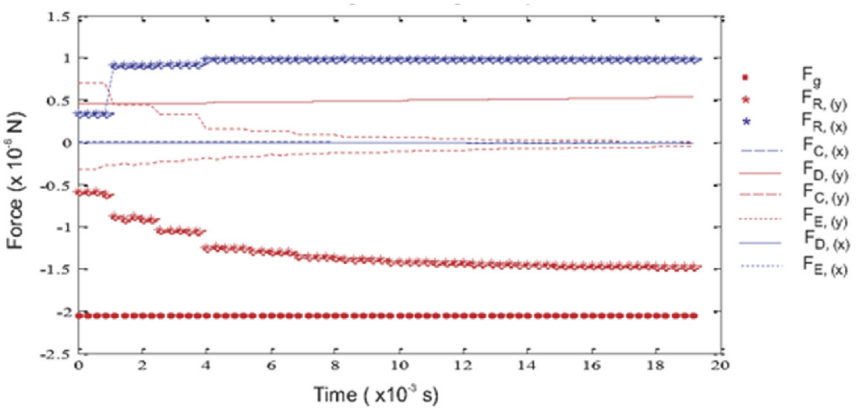


**Fig. 13.** A representation of all force components acting on a single droplet within a duration of 20 ms after their generation.

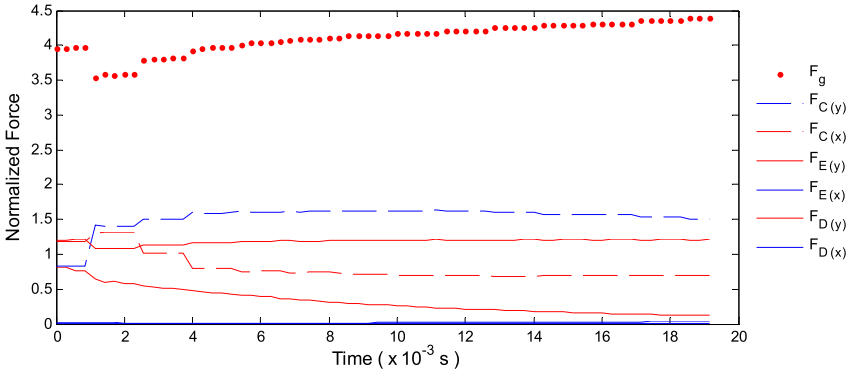


**Fig. 14.** Normalized weight of force components for all the considered droplets.

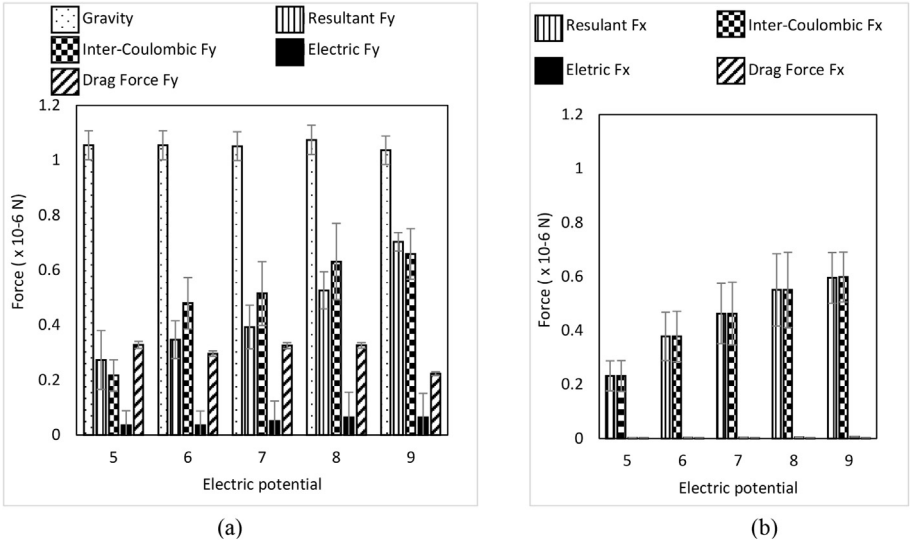


**Fig. 15.** A representation of the average magnitude of various force components acting on all the individual droplets within a duration of 20 ms after their generation; (a) axial component, (b) radial component. The error bars are for standard deviation.

In Fig. 15, the average magnitude of all force components acting on all the droplets for different values of applied electric potential at a flowrate of 285 mL $h^{-1}$ has been presented.

The analysis on the average magnitude of the forces acting on the droplets shows that the gravitational force, $\vec{F}_g$ has the highest average magnitude, followed by the coulombic force interaction, $\vec{F}_{C(x,y)}$, which plays a major role in dispersing the droplets as compared to electric field force, $\vec{F}_{E(x,y)}$.

## 4. Conclusions

A model describing the droplets' trajectories in the simple-jet

mode has been developed and validated. This model uses experimental (imaging) analysis to provide some input parameters, e.g. droplet initial velocity, break-up length, droplet diameter and deformation pattern. It also uses a support software to allow the calculation and implementation of the background electric field values, i.e. COMSOL Multiphysics®.

The 2D approach gave good agreement with the used validation technique (imaging technique). However, it is expected that a 3D approach would provide a more complete image of the droplet trajectories and final spray. Future experiments have thus to be performed both implementing a 3D environment to the model itself and to implement a 3D validation technique.

The initial hypothesis that the droplets' dispersion is initiated by their deformation was confirmed, both, by the experiments and the model. This is due to the displacement of their center of charge from their center of mass. Further, the theoretically adjusted droplets' charge was found to range between 2% and 4.5% of their Rayleigh limit, for the tested values of liquid flowrate (Q) and applied electric potential (Φ). These values are close to what was presented by Agostinho et al., 2012. However, independent experiments are recommended to measure the exact charge on the droplets in the Simple-Jet mode, which can be double-checked with the model.

The model also provides good insight into the various components of the different forces acting on the droplets. Thus it can be used to support decisions regarding the extra forces necessary to manipulate the droplets' trajectories.

## What is already known concerning the topic?

- Modes of Electrospraying, which produce monodisperse droplets have been identified as the Cone-Jet mode and the Simple-jet mode.
- The Cone-Jet mode is highly studied and various models have been proposed to describe the Taylor cone as well as the spray shape.
- The Simple-jet mode is not as highly explored as the Cone-Jet Mode.
- So far there has been no proposed model to describe the spray shape in the Simple-jet mode.
- The droplet charge can be expressed as a certain percentage of Rayleigh limit in the Simple-jet mode.

## Contributions for this paper

- Proposes a model that describes the spray shape in the Simple-jet mode for different values of liquid flow rate and applied electric potential.
- Discloses the mechanism that initiates the droplets' dispersion.
- Discloses the contribution of different components of force in determining the spray shape.
- Gives an insight into the kind of force that can be relied to manipulate the droplets' trajectories.
- Confirms that the droplet charge can be expressed as a certain percentage of Rayleigh limit in the Simple-jet mode.

## Funding

This work was supported by the Centre of Expertise Water Technology (CEW) and Waterhelp, both from Netherlands, as well as the International Science Program (ISP) from Sweden, through its Physics program in the University of Nairobi.

## Acknowledgement

We wish to express our gratitude to the management of the Water Application Centrum (WAC), for their relentless support while conducting our laboratory experiments. We also extend our sincere appreciation to Phill Citroën and Abhishek Rai for their contribution in carrying out experiments in the High Voltage Laboratory.

## References

[1] L.L.F. Agostinho, G. Taminga, C.U. Yurteri, S. Brouwer, E.C. Fuchs, J.C.M. Marijnissen, Morphology of water electrosprays in the simple-jet mode, Phy. Rev. E 066 (86) (2012) 317–326.
[2] W. Gilbert, De Magnete, London: Peter Short, 1600 (original Latin).
[3] R.P.A. Hartman, D.J. Brunner, D.M.A. Camelot, J.C.M. Marijnissen, B. Scarlett, The evolution of electrohydrodynamic sprays produced in the cone-jet mode, a physical model, J. Electrost. 47 (1999) 143–170.
[4] K.B. Geerse, Applications of Electrospray; from People to Plants, Technical University of Delft, 2003. PhD Thesis.
[5] K. Sung, C.S. Lee, Factor influencing liquid breakup in electrohydrodynamic atomization, J. Appl. Phys. 96 (7) (2004) 3956–3962.
[6] M.C. Kim, S.Y. Lee, Droplet formation under the spindle mode in electrohydrodynamic spraying-effects of nozzle material and flow rate, Proc. ILASS-Asia (2011) 229–234.
[7] M. Cloupeau, B. Prunet-Foch, Electrostatic spraying of liquids: main functioning modes, J. Electrost. 25 (2) (1990) 165–184.
[8] M. Cloupeau, B. Prunet-Foch, Electrohydrodynamic sparaying functioning modes: a critical review, J. Aerosol Sci. 25 (6) (1994) 1021–1036.
[9] J.M. Grace, J.C.M. Marijnissen, A review of liquid atomization by electrical means, J. Aerosal Sci. 25 (6) (1994) 1005–1019.
[10] J.M. Grace, P.F. Dunn, Droplet motion in an electrodynamic fine spray, J. Aerosol Sci. 20 (1996) 153–164.
[11] C.U. Yurteri, R.P.A. Hartman, J.C.M. Marijnissen, Producing pharmaceutical particles via electrospraying with an emphasis on nano and nano structured particles - a review, KONA Powder Part. J. 28 (2010) 91–115.
[12] A.M. Gañán-Calvo, J.C. Lasheras, J. Davila, A. Barrero, The electrostatic spray emitted from an electrified conical meniscus, J. Aerosol Sci. 25 (1994) 1121–1142.
[13] W.C. Hinds, Aerosol Technology; Properties,behaviour,and Measurement of Airborne Particles, John Wiley & Sons, Inc., New York, 1999.
[14] K. Tang, A. Gomez, On the structure of an electrostatic spray of monodisperse droplets, Phys. Fluids 6 (7) (1994) 2317–2332.
[15] J. Grifoll-Taverna, J. Rosell-Llompart, in: Modeling Electrospray Droplets Transport for Thin Film Formation, American Association for Aerosal Research (AAAR), Spain, 2009.
[16] L.L.F. Agostinho, Electrohydrodynamic Atomization in the Simple-jet Mode: Outscaling and Application, Technical University of Delft, The Hague, 2013. PhD Thesis.
[17] A. Gomez, K. Tang, Charge and fission of droplets in electrostatic sprays, Phys. Fluids A 6 (1994) 404–414.
[18] L. Agostinho, E. Fuchs, S. Metz, C. Yurteri, J. Marijnissen, Reverse movement and coalescence of water microdroplets in electrohydrodynamic atomization, Phys. Rev. E 84 (2) (2011) 026317.
[19] L.R. Grimm, J. Beauchamp, Dynamics of field induced droplet ionization: time-resolved studies of distortion, jetting, and progeny formation from charged and neutral methanol droplets exposed to strong electric fields, J. Phys. Chem. B 109 (16) (2005) 8244–8250.
[20] L. Agostinho, C. Yurteri, E.C. Fuchs, J. Marijnissen, Monodisperse water microdroplets generated by electrohydordynamic atomization in the simple-jet mode, Appl. Phys. Lett. 100 (24) (2012) 4.
[21] A. Gupta, S. M, Deformation and breakup of viscoelastic droplets in confined shear flow, Phys. Rev. E 90 (023305) (2014).
[22] H.B. Chin, C.D. Han, Studies on droplet deformation and breakup, J. Rheol. 23 (5) (1979) 557.
[23] E. Klaseboer, R. Manica, D. Chan, Universal behaviour of the initial stage of drop impact, Phys. Rev. Lett. 19 (194501) (2014) 113.
[24] S. Arash B, E. Mohsen D, A droplet deformation and breakup model based on virtual work principle, Phys. Fluids 27 (032103) (2015).
[25] L. Corson, C. Tsakonas, B. Duffy, N. Mottram, I. Sage, Deformation of a nearly hemispherical conducting drop due to an electric field: theory and experiment, Phys. fluids 26 (122106) (2014).
[26] H. David, R. Robert, W. Jearl, Fundamentals of Physics, John Wiley & Sons, Inc., New York, 1997.
[27] H.S. Fricker, Why does charge concentrate on points? Phys. Educ. U. K. 24 (1989) 157–161.
[28] R.P.A. Hartman, Electrohydrodynamic Atomization in the Cone Jet Mode. From Physical Modeling to Powder Technology, Technical University of Delft, The Hague, 1998. PhD Thesis.